



HAL
open science

Fabrication and characterization of a germanium nanowire light emitting diode

Johannes Greil, Emmerich Bertagnolli, Bassem Salem, Thierry Baron, Pascal Gentile, Alois Lugstein

► **To cite this version:**

Johannes Greil, Emmerich Bertagnolli, Bassem Salem, Thierry Baron, Pascal Gentile, et al.. Fabrication and characterization of a germanium nanowire light emitting diode. Applied Physics Letters, 2017, 111 (23), pp.233103. 10.1063/1.5006152 . cea-01988258

HAL Id: cea-01988258

<https://cea.hal.science/cea-01988258>

Submitted on 21 Jan 2019

HAL is a multi-disciplinary open access archive for the deposit and dissemination of scientific research documents, whether they are published or not. The documents may come from teaching and research institutions in France or abroad, or from public or private research centers.

L'archive ouverte pluridisciplinaire **HAL**, est destinée au dépôt et à la diffusion de documents scientifiques de niveau recherche, publiés ou non, émanant des établissements d'enseignement et de recherche français ou étrangers, des laboratoires publics ou privés.

Fabrication and characterization of a germanium nanowire light emitting diode

Johannes Greil¹, Emmerich Bertagnolli¹, Bassem Salem^{2,3}, Thierry Baron^{2,3}, Pascal Gentile⁴, Alois Lugstein^{1}*

¹ Institute of Solid State Electronics, TU Wien, Floragasse 7, 1040 Vienna, Austria

² Université de Grenoble Alpes, LTM, F-38000 Grenoble, France

³ CNRS, LTM, F-38000 Grenoble, France

⁴ CEA, INAC-PHELIQS, 17 rue des Martyrs, F-38000 Grenoble, France

Abstract

In this letter we demonstrate the feasibility of a germanium nanowire light emitting diode as a reasonable approach for downscaling of CMOS compatible light sources. We show room-temperature direct bandgap electroluminescence from axial p-n junction nanowire devices. The electron population in the Γ valley, necessary for direct bandgap emission, is achieved by high injection current densities. Carrier temperature is consistently found to be higher than the lattice temperature, indicating inhibited carrier cooling in small diameter wires. Strong polarization of the emission parallel to the nanowire axis is observed and attributed to dielectric contrast phenomena.

¹Corresponding author. Email: alois.lugstein@tuwien.ac.at

The ongoing scaling of CMOS technology and thus conceivable limitations of common metallization schemes, demands for silicon-compatible light sources, transmitters and detectors for on-chip communication and triggered enormous research activities in group IV semiconductor photonics.^{1,2} Thereby novel light generation schemes like Raman lasers³, photonic crystals⁴, quantum dots⁵, and erbium doping⁶ have already been demonstrated. From the material side germanium (Ge) is highlighted amongst the group IV materials due to its quasidirect nature with the conduction band minimum at the Γ -point only 140meV higher in energy than the minimum at the L-point. Beneficially, the direct bandgap energy of Ge translates to an emission wavelength in the telecommunication band of 1550nm. Moreover, it has already been demonstrated that the emission properties of Ge may be tailored by utilizing quantum confinement⁷, strain engineering^{8,9}, n-type doping¹⁰, alloying with Sn¹¹, tuning of the temperature¹² or combinations thereof. Planar Ge LEDs¹²⁻¹⁶ as well as optically¹⁰ and electrically¹⁷ pumped Ge lasers have recently been demonstrated in devices with dimensions on the micron scale. Following the route of downscaling, nanowire (NW) based devices are a next logical step. However, so far only III-V materials have been employed in axial p-n junction LED devices¹⁸⁻²¹. Here we present room temperature electroluminescence (EL) from Ge NW axial p-n diodes with a junction area of less than $0.01\mu\text{m}^2$. A bottom-up approach is pursued, with the potential for versatile integration of NW functional building blocks in various device architectures.

Ge NWs were synthesized in a low pressure chemical vapor deposition chamber with GeH₄ (50sccm of 10% GeH₄ in H₂) as a precursor gas at a growth temperature of T=673K and a total chamber pressure of 12.8mbar. The vapor-liquid-solid growth mechanism²² was employed to achieve axial p-n junction NWs with Au colloids as growth catalyzing particles. The p- and n-type segments are defined by introducing B₂H₆ (B₂H₆/GeH₄ ratio = 2×10^{-2}) and PH₃ (PH₃/GeH₄ ratio = 3×10^{-2}) into the growth chamber, respectively resulting in electrically active doping densities of about 10^{19} at.cm⁻³ determined by four probe measurements.

Uncatalytic deposition on the NW sidewalls during the growth at this rather high temperature leads to strongly tapered NWs enabling efficient outcoupling of light.²³ However, the unintentional deposition of n-type material on the sidewalls of the foremost grown p-type section of the NW, potentially bypasses the p-n junction electrically²⁴ (see Figure 1a). Remarkably, as will be shown later, selective etching of this unintentional n-type layer greatly improves the electrical diode properties, whereas the optical emission properties are not altered significantly. To fabricate devices as shown in the SEM image in Figure 1a, the p-n junction NWs were removed from the growth substrate and deposited via mechanical transfer on a highly doped substrate covered by silicon oxide. Electrical contacts to individual NWs were established by electron beam lithography, Ni/Au sputter deposition and lift-off techniques. In agreement with literature we observed ohmic contacts to both highly doped p- and n-type Ge segments.²⁵

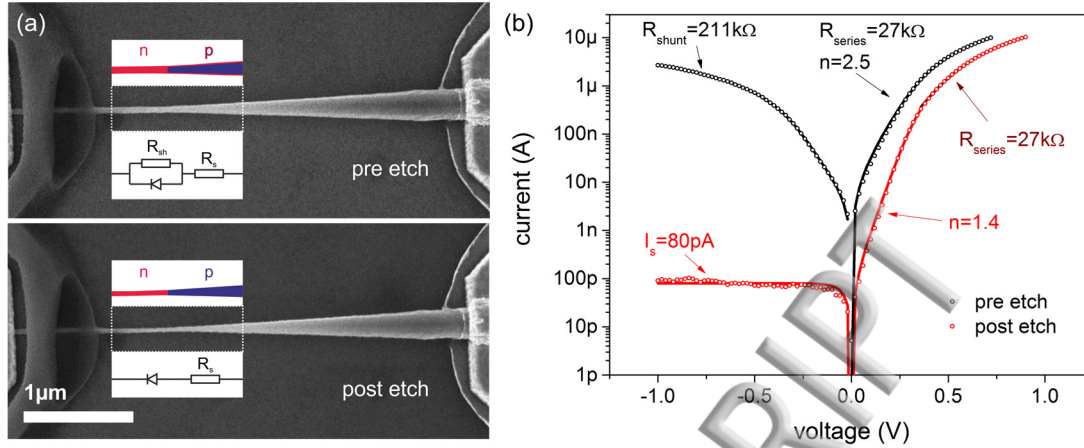


Figure 1. Ge p-n junction NW device. (a) SEM images of the Ge p-n NW, together with a sketch of the p- and n-type regions of the device and a sketch of the equivalent circuits before and after etching of the parasitic n-doped Ge layer. (b) I/V characteristics before (black) and after (red) the etching procedure. Open circles are measured data points, solid lines are fits to the data according to eq. 1. The parasitic shunt disappears after the n-Ge layer removal, while the series resistance stays roughly the same. The diode ideality factor improves from 2.5 to 1.4.

NW diodes were electrically characterized and the I/Vs fitted according to the diode equation:

$$I = I_s \left[\exp\left(\frac{q(V - IR_s)}{nk_B T}\right) - 1 \right] + \frac{q(V - IR_s)}{R_{sh}} \quad (\text{eq. 1})$$

with I_s the diode saturation current, q the elementary charge, R_s the series resistance, k_B the Boltzmann constant, n the ideality factor, T the temperature, and R_{sh} the resistance of the parasitic shunt (see Figure 1a). Electrical characterization of the as-grown NWs reveals the expected high reverse current due to shunting of the p-n junction by the unintentional deposited n-type layer (Figure 1b). A 30s dip in deionized water at room temperature is employed to remove the n-type Ge layer. The NW diameter in the n-type region is thereby reduced from $\sim 57\text{nm}$ to $\sim 33\text{nm}$ on average. After etching, diode characteristics are greatly improved and current rejection ratios as high as 10^5 are obtained. The shunt resistance that is estimated around $211\text{k}\Omega$ for the as-grown NWs

completely disappears, while the series resistance of around 27k Ω is not affected and the diode ideality factor improves from n=2.5 to n=1.4.

To gain further insight into the internal electric field distribution along the axial p-n NW junction, scanning photocurrent spectroscopy was employed (Figure 2).²⁶ Therefore the short-circuit current of the Ge NW device was recorded while a focused laser beam was scanned along the NW.

For NWs under certain constraints discussed by Allen et al.²⁷ the photocurrent I_{ph} is expected to be proportional to the local electric field. Assuming further that the absorption strength along the tapered NWs is constant, the effective electrostatic potential profile Φ_{eff} along the NW can be determined according to

$$\phi_{eff} \propto \int I_{ph}(x) dx \quad (\text{eq. 2})$$

Independent of the excitation power P_{exc} , the position of the p-n junction is clearly determined in the electrostatic potential profile, while the potential in the vicinity of the (left) p-type contact is completely flat. Close to the (right) n-type contact there are indications of a Schottky barrier induced field, though negligible compared to the p-n junction related field.

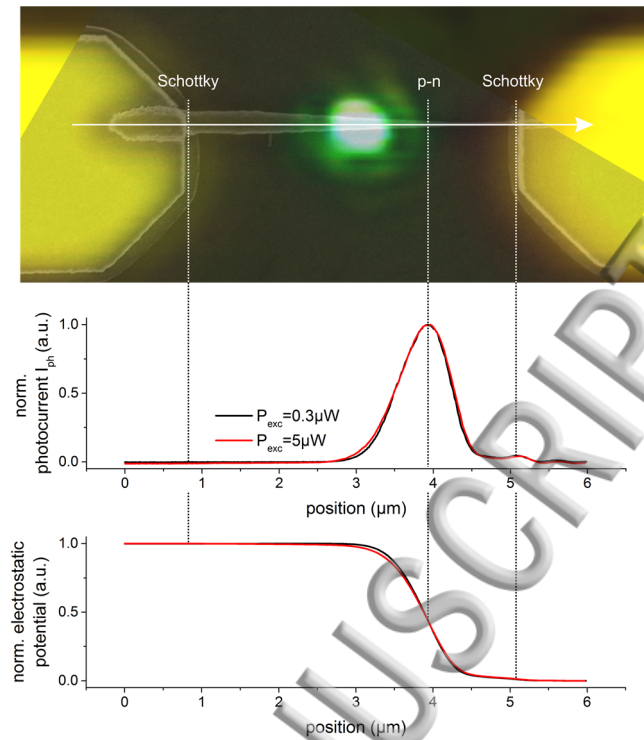


Figure 2. Scanning photocurrent spectroscopy. The uppermost panel shows an overlay of an optical image with the excitation laser spot and an SEM image of the etched NW. Independent of the excitation power, the photocurrent scales with the internal electric field and is highest at the p-n junction, linescans along the NW axis provide the exact position of the junction. The electrostatic potential profile reveals negligible Schottky barriers at the metal-semiconductor contacts. The lowermost panel shows the thereof calculated profile of the effective electrostatic potential.

To elucidate the electro-optical properties of the axial p-n junction Ge NW device, the forward bias was varied between 0.4V to 0.8V and representative EL spectra were collected as a function of the injection current through the NW. Figure 3a shows exemplarily the near-infrared spectra down to an energy of 0.78eV, limited by the InGaAs detector sensitivity. The current density in the tapered NWs was calculated by normalizing the device current to the cross-sectional area in the small-diameter n-type region that provides the bottle neck for electrical current.

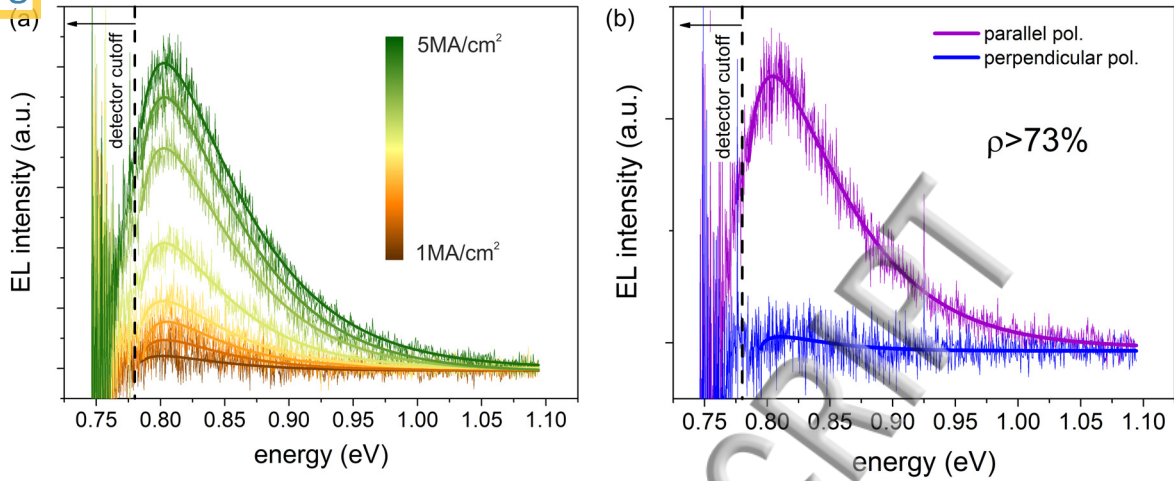


Figure 3. Room temperature EL of the Ge NW p-n diode biased in forward direction. (a) EL spectra for increasing current density, (b) Polarization dependence of the emission. A high degree of polarization >73% was found. Solid lines in both panels are fits to the Maxwell-Boltzmann distribution.

Due to the limitations in detector range we can only observe the direct bandgap transition, expected at ~0.8eV at room temperature²⁸. The spectra are fitted according to the Maxwell-Boltzmann distribution²⁹ for spontaneous direct bandgap recombination:

$$I_{EL} \propto \sqrt{h\nu - E_{g,d}} \exp\left(-\frac{h\nu - E_{g,d}}{k_B T_C}\right) \quad (\text{eq. 3})$$

with h Planck's constant, ν the optical frequency, $E_{g,d}$ the direct bandgap of Ge and T_C the carrier temperature. Furthermore, the polarization properties of the emission are plotted in Figure 3b. Strong polarization of the EL is observed along the NW axis with a degree of polarization of about $\rho > 73\%$. A high degree of polarization along the NW axis is frequently reported for cubic semiconductors^{30,31} and can be understood in terms of the dielectric contrast of the NW and its surroundings.³² For an electric field polarized parallel

For the Ge NW, the field E_i inside the NW equals the field E_e outside ($E_i = E_e$). For perpendicular polarization, though, the field inside is highly attenuated:

$$E_i = \frac{2\varepsilon_0}{\varepsilon + \varepsilon_0} E_e \quad (\text{eq. 4})$$

with the dielectric constant for Ge of $\varepsilon=16.2$ and the dielectric constant of air $\varepsilon_0=1$. A theoretical polarization ratio of $\rho=97\%$ is expected, even higher than what is experimentally observed. Additionally, leaky-mode resonances confining light within sub-wavelength nanostructures exhibit a steep diameter dependency of the TM/TE polarization ratio.³³ Due to the tapering of the p-n NW devices, however, a complex mode profile may be expected and thus the degree of polarization is not predictable in a straight forward way.

The EL emission properties were investigated of as grown NWs as well as after the removal of the parasitic n-doped shell. Figure 4 shows parameters extracted from fits to the spectra according to eq. 3 before and after the etching procedure. The lattice temperature is estimated employing two independent approaches. First, temperature is extracted by employing Varshni's law and the bandgap energy $E_{g,d}$.

$$E_{g,d} = E_0 - \frac{\alpha T^2}{T + \beta} \quad (\text{eq. 5})$$

with $E_0=0.89\text{eV}$ the bandgap at $T=0\text{K}$, $\alpha=5.82*10^{-4}\text{eV/K}^2$, $\beta=296\text{K}$.²⁸ Second, Raman characterization of the NW junction region is employed and we estimate the lattice

temperature via the Raman shift of the main optical phonon peak^{34,35} according to the linearization $\Delta T = k \cdot \Delta\Omega$ with ΔT the temperature and $\Delta\Omega$ the Raman peak shift. The linear factor $k=62.3\text{K/rel.cm}^{-1}$ was determined from a temperature dependent study.³⁴ The temperature of the charge carrier was extracted by fitting the high-energy wing of the electroluminescence spectra.³⁶ The lattice temperature estimated from Raman characterization appeared to be slightly lower than the lattice temperature estimated from the temperature dependency of the bandgap energy. We can speculate that locally within the recombination region the temperature is higher than derived from Raman characterization at the junction position. In these hot-spots recombination probability is higher and thus the emission from localized regions with increased temperature could dominate the emission. Considering the lattice temperature from both approaches, Joule heating is slightly increasing the temperature of the lattice with increasing current density. However in this temperature regime we can exclude thermal radiation as a source of emission in the considered range. The peak wavelength and total radiated amount of a thermal emitter vary with temperature according to Wien's displacement law. Emission with a maximum at about $1.5\mu\text{m}$ corresponds thus to a temperature of about 1200K, far above the temperature we determined for our light emitting device and even above the melting temperature of Ge.

Overall for all devices we observe a significantly higher carrier temperature of $\approx 550\text{K}$ as compared to the lattice temperature of $\approx 350\text{K}$ at high injection current, indicating non-equilibrium hot-carrier recombination. Similar to the observed behavior, carrier temperature has been frequently reported to be higher than the actual junction temperature in common planar LED structures.³⁶ Proposed mechanisms are Auger

combination, intervalence band absorption³⁷ or high-energy carrier injection in the active region under large forward bias³⁸. Particularly for NWs, a recent work of Tedeschi et al.³⁹ has addressed the role of inhibited phonon emission in confined nanostructures for hot-carrier luminescence. Therein, a general trend of increasing carrier temperature with decreasing NW diameter was found under *quasi-equilibrium* conditions provided by continuous wave excitation. The proposed mechanism relates to effective phonon scattering at the NW surface, preventing the carriers from reaching thermal equilibrium with the lattice via phonon emission. Qualitatively this trend is reproduced in Figure 4b, since the etched NWs tend to exhibit a higher carrier temperature than the as-grown NWs with larger diameter.

ACCEPTED MANUSCRIPT

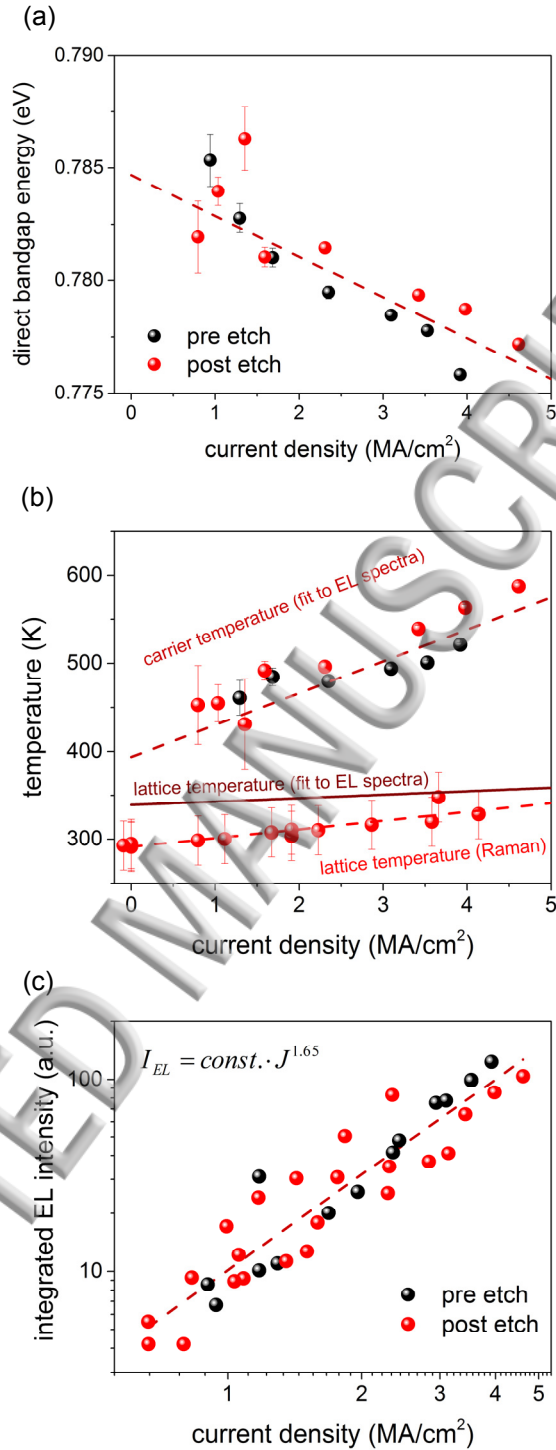


Figure 4. Bandgap energy, temperature, and EL intensity as a function of current density. Direct bandgap energy, carrier temperature and integrated intensity are extracted from fits to the EL spectra. Black spheres correspond to as-grown NWs, red spheres to the NWs after the etching procedure. Lines represent linear fits. (a) The direct bandgap energy decreases due to Joule heating of the lattice. (b) Carrier and lattice temperature are increasing. Lattice temperature is derived in two independent ways, from Raman

characterization and from the bandgap values shown in (a) using Varshni's equation. (c) Integrated EL intensity as a function of current density on a log-log scale follows a power law with exponent $k=1.65$.

Figure 4c shows the integrated EL intensity as a function of current density. The linear relationship in the log-log plot indicates a power law $I_{EL} \propto J^k$ with the exponent $k=1.65$. The intensity dependence compares well with published values of planar Ge LEDs ranging from $k=1.48 - 2$.^{15,40,41} A superlinear increase of EL intensity with current density has been proposed to be related to an increased efficiency of the direct bandgap transition due to (i) an increased ratio of direct to indirect states with high injection⁴¹, (ii) Joule heating¹⁵ and (iii) band-filling of the L valley¹⁴. At increased temperatures the Fermi distribution widens and at higher injection the electron quasi Fermi level rises, thus increasing the density of electrons populating the Γ valley.

Summarizing, we have presented direct bandgap emission from electrically pumped Ge NW p-n diodes. The EL is dominated by hot-carrier recombination, supposedly due to inhibited phonon emission in smaller diameter NWs. A superlinear dependency of the EL intensity on current density is in agreement with previously published data for planar Ge LEDs. The realized downscaling of a CMOS compatible light source to the nanoscale could be of great relevance for envisaged on-chip group IV photonics applications.

Acknowledgements

The authors gratefully acknowledge financial support by the Austrian Science Fund (FWF): project No.: P28175-N27. The authors further thank the Center for Micro- and Nanostructures for providing the cleanroom facilities.

References

- (1) R. Geiger, T. Zabel, H. Sigg, *Front. Mater.* **2**, 52.(2015)
- (2) L. Tsybeskov, D. J. Lockwood, *Proc. IEEE* **97**, 7, 1284 (2009)
- (3) H. Rong, A. Liu, R. Jones, O. Cohen, D. Hak, R. Nicolaescu, A. Fang, M. Paniccia, *Nature* **433**, 292 (2005)
- (4) X. Checoury, M. El Kurdi, Z. Han, P. Boucaud, *Opt. Express* **17**, 5, 3500 (2009)
- (5) L. Pavesi, L. Dal Negro, C. Mazzoleni, G. Franzò, F. Priolo, *Nature* **408**, 440 (2000)
- (6) L. Dal Negro, R. Li, J. Warga, S. N. Basu, *Appl. Phys. Lett.* **92**, 181105 (2008)
- (7) J. Xia, T. Maruizumi, Y. Shiraki, *Front. Optoelectron.* **5**, 1, 13 (2012)
- (8) M. El Kurdi, G. Fishman, S. Sauvage, P. Boucaud, *J. Appl. Phys.* **107**, 013710 (2010)
- (9) M. J. Süess, R. Geiger, R. A. Minamisawa, G. Schiefler, J. Frigerio, D. Chrastina, G. Isella, R. Spolenak, J. Faist, H. Sigg, *Nat. Photonics* **7**, 466 (2013)
- (10) J. Liu, X. Sun, R. Camacho-Aguilera, L. C. Kimerling, J. Michel, *Opt. Lett.* **35**, 5, 679 (2010)
- (11) S. Wirths, Z. Ikonc, A.T. Tiedemann, B. Holländer, T. Stoica, G. Mussler, U. Breuer, J.M. Hartmann, A. Benedetti, S. Chiussi, D. Grützmacher, S. Mantl, D. Buca, *Appl. Phys. Lett.* **103**, 192110 (2013)
- (12) T.-H. Cheng, C.-Y. Ko, C.-Y. Chen, K.-L. Peng, G.-L. Luo, C. W. Liu, H.-H. Tseng, *Appl. Phys. Lett.* **96**, 9, 091105 (2010)
- (13) W. Hu, B. Cheng, C. Xue, H. Xue, S. Su, A. Bai, L. Luo, Y. Yu, Q. Wang, *Appl. Phys. Lett.* **95**, 092102 (2009)
- (14) X. Sun, J. Liu, L. C. Kimerling, J. Michel, *Opt. Lett.* **34**, 8, 1198 (2009)

- (15) S.-L. Cheng, J. Lu, G. Shambat, H.-Y. Yu, K. Saraswat, J. Vuckovic, Y. Nishi, *Opt. Express* **17**, 12, 10019 (2009)
- (16) M. de Kersauson, R. Jakomin, M. El Kurdi, G. Beaudoin, N. Zerounian, F. Aniel, S. Sauvage, I. Sagnes, P. Boucaud, *J. Appl. Phys.* **108**, 023105 (2010)
- (17) R. E. Camacho-Aguilera, Y. Cai, N. Patel, J. T. Bessette, M. Romagnoli, L. C. Kimerling, J. Michel, *Opt. Express*, **20**, 10, 11316 (2012)
- (18) K. Haraguchi, T. Katsuyama, K. Hiruma, K. Ogawa, *Appl. Phys. Lett.* **60**, 745–747 (1992)
- (19) M. S. Gudiksen, L. J. Lauhon, J. Wang, D. C. Smith, C. M. Lieber, *Nature* **415**, 617 (2002)
- (20) H. M. Kim, Y.-H. Cho, H. Lee, S. I. Kim, S. R. Ryu, D. Y. Kim, T. W. Kang, K. S. Chung, *Nano Lett.* **4**, 6, 1059 (2004)
- (21) E. D. Minot, F. Kelkensberg, M. van Kouwen, J. A. van Dam, L. P. Kouwenhoven, V. Zwiller, M. T. Borgström, O. Wunnicke, M. A. Verheijen, E. P. Bakkers, *Nano Lett.* **2007**, 7, 2, 367 (2007)
- (22) R. S. Wagner, W. C. Ellis, *Appl. Phys. Lett.* **4**, 89 (1964)
- (23) I. Friedler, C. Sauvan, J. P. Hugonin, P. Lalanne, J. Claudon, J. M. Gérard, *Opt. Express* **17** (4), 2095 (2009)
- (24) K. Guilloy, N. Pauc, A. Gassenq, P. Gentile, S. Tardif, F. Rieutord, V. Calvo, *Nano Lett.* **15**, 2429 (2015)
- (25) S. T. Le, P. Jannaty, A. Zaslavsky, S. A. Dayeh, S. T. Picraux, *Appl. Phys. Lett.* **96**, 262102 (2010)
- (26) J. Greil, S. Birner, E. Bertagnolli, A. Lugstein, *Appl. Phys. Lett.* **104**, 163901 (2014)
- (27) J. E. Allen, D. E. Perea, E. R. Hemesath, L. J. Lauhon, *Adv. Mater.* **21**, 3067 (2009)

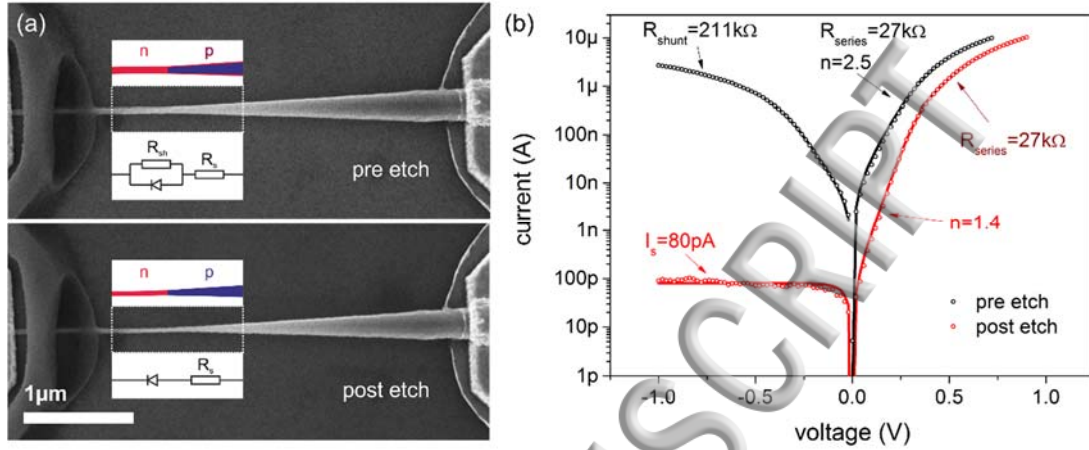
- (28) *Handbook Series on Semiconductor Parameters; Levinshtein, M., Rumyantsev, S., Shur, M., Eds.; World Scientific, 1996.*
- (29) N. C. Chen, W. C. Lien, Y. K. Yang, C. Shen, Y. S. Wang, J. F. Chen, *J. Appl. Phys.* **106**, 074514 (2009)
- (30) R. Agarwal, C. M. Lieber, *Appl. Phys. A* **85**, 209 (2006)
- (31) A. Mishra, L. V. Titova, T. B. Hoang, H. E. Jackson, L. M. Smith, J. M. Yarrison-Rice, Y. Kim, H. J. Joyce, Q. Gao, H. H. Tan, C. Jagadish, *Appl. Phys. Lett.* **91**, 263104 (2007)
- (32) J. Wang, M. S. Gudixsen, X. Duan, Y. Cui, C. M. Lieber, *Science* **293**, 1455 (2001)
- (33) L. Cao, J. S. White, J.-S. Park, J. A. Schuller, B. M. Clemens, M. L. Brongersma, *Nat. Mater.* **8**, 643 (2009)
- (34) A. Lugstein, M. Mijić, T. Burchhart, C. Zeiner, R. Langegger, M. Schneider, U. Schmid, E. Bertagnolli, *Nanotechnology* **24**, 065701 (2013)
- (35) G. S. Doerk, C. Carraro, R. Maboudian, *Phys. Rev. B* **80**, 073306 (2009)
- (36) S. Chhajed, Y. Xi, Y.-L. Li, T. Gessmann, E. F. Schubert, *J. Appl. Phys.* **97**, 054506 (2005)
- (37) J. Shah, R. F. Leheny, R. E. Nahory, H. Temkin, *Appl. Phys. Lett.* **39**, 618 (1981)
- (38) Y. Xi, J.-Q. Xi, T. Gessmann, J. M. Shah, J. K. Kim, E. F. Schubert, A. J. Fischer, M. H. Crawford, K. H. A. Bogart, A. Allerman, *Appl. Phys. Lett.* **86**, 031907 (2005)
- (39) D. Tedeschi, M. De Luca, H. A. Fonseka, Q. Gao, F. Mura, H. H. Tan, S. Rubini, F. Martelli, C. Jagadish, M. Capizzi, A. Polimeni, *Nano Lett.* **16**, 5, 3085 (2016)
- (40) M. Kaschel, M. Schmid, M. Gollhofer, J. Werner, M. Oehme, J. Schulze, *Solid. State. Electron.* **83**, 87 (2013)
- (41) E. Kasper, M. Oehme, J. Werner, T. Aguirov, M. Kittler, *Front. Optoelectron.* **5**, 3, 256

ACCEPTED MANUSCRIPT

Figure 1:



This manuscript was accepted by Appl. Phys. Lett. Click [here](#) to see the version of record.



ACCEPTED MANUSCRIPT



Figure 2:

This manuscript was accepted by Appl. Phys. Lett. Click [here](#) to see the version of record.

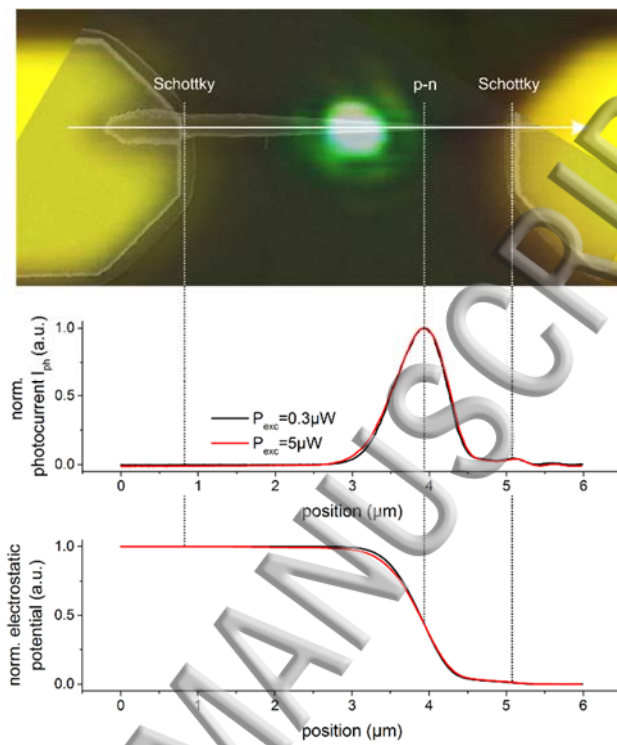
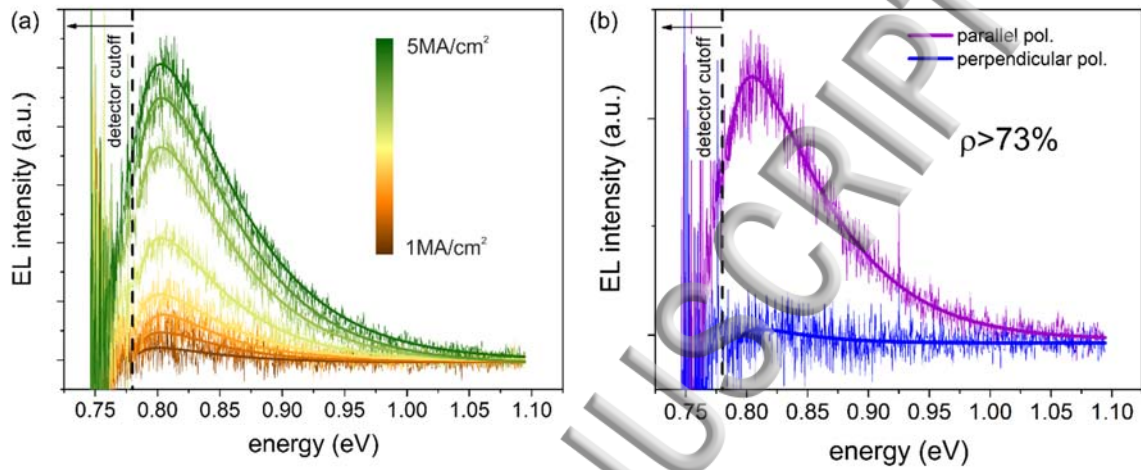




Figure 3:

This manuscript was accepted by Appl. Phys. Lett. Click [here](#) to see the version of record.



ACCEPTED MANUSCRIPT



Figure 4:

This manuscript was accepted by Appl. Phys. Lett. Click [here](#) to see the version of record.

